

Confined states in two-dimensional flat elliptic quantum dots and elliptic quantum wires

M. van den Broek and F. M. Peeters*

Departement Natuurkunde, Universiteit Antwerpen, Universiteitsplein 1, B-2610

Antwerpen, Belgium

(23 March 2001)

Abstract

The energy spectrum and corresponding wave functions of a flat quantum dot with elliptic symmetry are obtained exactly. A detailed study is made of the effect of ellipticity on the energy levels and the corresponding wave functions. The analytical behavior of the energy levels in certain limiting cases is obtained.

PACS numbers: 03.65.Ge, 73.21.La

Keywords: quantum dot, elliptic, ellipse

I. INTRODUCTION

Quantum dots have been the subject of both experimental and theoretical research in recent years [1]. They have been successfully created experimentally by applying lithographic and etching techniques to impose a lateral structure onto an otherwise two-dimensional electron system. These structures introduce electrostatic potentials in the plane of the two-dimensional electron gas, which confine the electrons to a dot region. The energy levels of electrons in such a quantum dot are fully quantized like in an atom, and therefore they are also referred to as *artificial atoms*. For a theoretical description of such systems it is essential to know the confinement potential. Often a parabolic potential is used. Another simple model, which also has the advantage of representing a finite confinement, is a piecewise constant potential with a circular boundary [2]. This type of potential represents more closely the situation in self-assembled quantum dots [1]. The latter model is used, but extended to an asymmetric situation, i.e. an elliptic dot.

There have been many calculations of energy levels in rectangular dots and wires, see for example [3–5], but in general, the problem of even one particle confined in such a potential profile is not exactly solvable, because the corresponding Schrödinger equation is not separable. Nevertheless one usually assumes separability, although this approximation is only acceptable for deep wells, where only a negligible part of the wave function is situated outside the dot. In our study we use an elliptically shaped potential profile for which exact solutions can be found, even when we take $\Psi|_{\text{interface}} \neq 0$, or a potential $V_0 \ll \infty$ outside the dot. We are especially interested in the results for elongated dots, which could then be

compared with the case of a rectangular slab or even a quantum wire. Our results are also applicable to elliptic quantum wires.

In the literature one can find many references to calculations on elliptic problems, we found one particularly useful [6], in which the diffraction of waves by ribbons and by slits is studied exactly. The problem of a three-dimensional ellipsoidal (3D) quantum well has been solved exactly in Refs. [7] and [8] for $\Psi|_{\text{interface}} = 0$. To our knowledge, the corresponding 2D problem for finite potential barriers has not been solved.

The paper is organized as follows. In Sec. II, we obtain the analytical solution for the energy and the wave functions. The numerical results are presented in Sec. III. Our conclusions are given in Sec. IV. A representation for the Mathieu functions is listed in the appendix.

II. THE PROBLEM AND EQUATIONS

A particle with mass m is confined in a two-dimensional hard-wall potential well of finite height with elliptic shape as shown in Fig. 1. The potential profile we consider is constant everywhere, $V(x, y) = 0$ inside the dot (i.e. $x^2/a^2 + y^2/b^2 < 1$) and $V(x, y) = V_0$ outside the dot. Stationary energy levels and wave functions are found by solving the time-independent Schrödinger equation

$$-\frac{\hbar^2}{2m}\nabla^2\Psi(x, y) + V(x, y)\Psi(x, y) = E\Psi(x, y). \quad (1)$$

Transformation from Cartesian to elliptical coordinates $x = f \cosh u \cos v$, $0 \leq u \leq \infty$, $y = f \sinh u \sin v$, $0 \leq v \leq 2\pi$, where $f = \sqrt{a^2 - b^2}$ is the focal length, enables us to write the boundary of the ellipse in a one-variable equation $u = U = \text{arctanh}(b/a)$. Introducing the electron momentum $k^2 = \frac{2m}{\hbar^2}(E - V)$ the equation to be solved becomes

$$\frac{\partial^2\Psi}{\partial u^2} + \frac{\partial^2\Psi}{\partial v^2} + \frac{f^2k^2}{2} \cosh 2u \Psi - \frac{f^2k^2}{2} \cos 2v \Psi = 0. \quad (2)$$

Proposing a solution $\Psi(u, v) = F(u)G(v)$ we find that the problem is separable in two equations in u and v , coupled by a separation constant c and the variable k . Denoting $q = f^2k^2/4$ we obtain,

$$\frac{d^2F(u)}{du^2} - (c - 2q \cosh 2u)F(u) = 0, \quad (3a)$$

$$\frac{d^2G(v)}{dv^2} + (c - 2q \cos 2v)G(v) = 0, \quad (3b)$$

which are the characteristic equations for the Mathieu functions. Physical solutions to these equations are well-known [14]

$$G_l(v, q) = \begin{cases} \text{ce}_l(v, q), \\ \text{se}_l(v, q), \end{cases} \quad (4a)$$

$$F_l^{\text{in}}(u, q) = \begin{cases} \text{Mc}_l^{(1)}(u, q_1), \\ \text{Ms}_l^{(1)}(u, q_1), \end{cases} \quad (4b)$$

$$F_l^{\text{out}}(u, q) = \begin{cases} \text{Mc}_l^{(3)}(u, -q_2), \\ \text{Ms}_l^{(3)}(u, -q_2), \end{cases} \quad (4c)$$

where $l = 0, 1, 2, \dots$. The normalization factors are discarded and will be incorporated later in the total wave function $\Psi(u, v)$. The Mathieu functions $ce_l(v, q)$ and $se_l(v, q)$ are respectively even and odd in v and are the analogue of the cosine and sine functions in the angular solution of the circular dot problem. For the u -problem we make a distinction between solutions inside and outside the dot. The former show oscillatory behavior and are the analogue of the Bessel functions $J_l(\rho)$ in the radial solution of the circular problem. The latter are monotonically decaying functions and are the analogue of the modified Bessel functions $K_l(\rho)$ in the circular problem. In choosing these particular functions we used the boundary conditions that the wave functions need to be finite when $u = 0$ and $u \rightarrow \infty$ for obvious normalization reasons. Outside the dot $E < V_0$ and the variable q becomes negative, which we noted explicitly. In the appendix explicit expressions for the Mathieu functions are given.

The wave function $\Psi(u, v)$ and its derivatives must be continuous everywhere. This condition requires that at every point on the border (U, v) of the quantum dot we have

$$\frac{\partial F_l^{\text{in}}(u, q)/\partial u|_{u=U, q=q_1}}{F_l^{\text{in}}(U, q_1)} = \frac{\partial F_l^{\text{out}}(u, q)/\partial u|_{u=U, q=-q_2}}{F_l^{\text{out}}(U, -q_2)}, \quad (5)$$

where the u -independent functions $G_l(v, q)$ cancel out.

We introduce $\sigma = \sqrt{ab}$, which is related to the area of the ellipse and define

$$\xi = \sigma k_1, \quad \eta = \sigma k_2, \quad \gamma = \sigma \sqrt{\frac{2m}{\hbar^2} V_0}, \quad (6)$$

with $k_1^2 = \frac{2m}{\hbar^2} E$ and $k_2^2 = \frac{2m}{\hbar^2} (V_0 - E)$. The energy levels will be expressed in units of V_0 . Clearly $\xi^2 + \eta^2 = \gamma^2$ and $q_1 = \frac{f^2 k_1^2}{4} = \frac{1}{4} \frac{f^2}{\sigma^2} \xi^2 = \frac{1}{4} \left(\frac{a}{b} - \frac{b}{a}\right) \xi^2$. We are therefore left with two equations for even and odd solutions in one variable ξ to be solved numerically

$$\frac{\partial \text{Mc}_l^{(1)} / \partial u \left(u, \frac{1}{4} \left(\frac{a}{b} - \frac{b}{a}\right) \xi^2 \right) \Big|_{u=U}}{\text{Mc}_l^{(1)} \left(U, \frac{1}{4} \left(\frac{a}{b} - \frac{b}{a}\right) \xi^2 \right)} = \frac{\partial \text{Mc}_l^{(3)} / \partial u \left(u, -\frac{1}{4} \left(\frac{a}{b} - \frac{b}{a}\right) (\gamma^2 - \xi^2) \right) \Big|_{u=U}}{\text{Mc}_l^{(3)} \left(U, -\frac{1}{4} \left(\frac{a}{b} - \frac{b}{a}\right) (\gamma^2 - \xi^2) \right)}, \quad (7a)$$

$$\frac{\partial \text{Ms}_l^{(1)} / \partial u \left(u, \frac{1}{4} \left(\frac{a}{b} - \frac{b}{a}\right) \xi^2 \right) \Big|_{u=U}}{\text{Ms}_l^{(1)} \left(U, \frac{1}{4} \left(\frac{a}{b} - \frac{b}{a}\right) \xi^2 \right)} = \frac{\partial \text{Ms}_l^{(3)} / \partial u \left(u, -\frac{1}{4} \left(\frac{a}{b} - \frac{b}{a}\right) (\gamma^2 - \xi^2) \right) \Big|_{u=U}}{\text{Ms}_l^{(3)} \left(U, -\frac{1}{4} \left(\frac{a}{b} - \frac{b}{a}\right) (\gamma^2 - \xi^2) \right)}. \quad (7b)$$

Solutions are indexed $\xi_{n,l}$, $n = 1, 2, \dots$; $l = 0, 1, \dots$. The energy spectrum is then given by

$$E_{n,l} = \frac{\hbar^2}{2m} k_{1n,l}^2 = \frac{\xi_{n,l}^2}{\gamma^2} V_0. \quad (8)$$

In the limit of an infinitely high barrier, $V_0 \rightarrow \infty$, the boundary condition will simply become $F_l^{\text{in}}(u = U, q_1) = 0$, or equivalently,

$$\text{Mc}_l^{(1)} \left(U, \frac{1}{4} \left(\frac{a}{b} - \frac{b}{a}\right) \xi^2 \right) = 0, \quad (9a)$$

$$\text{Ms}_l^{(1)} \left(U, \frac{1}{4} \left(\frac{a}{b} - \frac{b}{a}\right) \xi^2 \right) = 0. \quad (9b)$$

When the particle has a different effective mass inside (m_1) and outside the dot (m_2) the boundary condition Eq. (5) has to be modified into

$$\frac{\partial F_l^{\text{in}}/\partial u(u, q_1)|_{u=U}}{m_1 F_l^{\text{in}}(U, q_1)} = \frac{\partial F_l^{\text{out}}/\partial u(u, -q_2)|_{u=U}}{m_2 F_l^{\text{out}}(U, -q_2)}. \quad (10)$$

The explicit expressions for the wave functions are, for the even functions,

$$\Psi_{n,l}^e(u, v) = \begin{cases} N_{n,l}^e \text{Mc}_l^{(1)}(u, q_{1,n,l}) \text{ce}_l(v, q_{1,n,l}), & u \leq U, \\ N_{n,l}^e \text{Mc}_l^{(3)}(u, -q_{2,n,l}) \text{ce}_l(v, -q_{2,n,l}), & u > U, \end{cases} \quad (11)$$

and for the odd functions,

$$\Psi_{n,l}^o(u, v) = \begin{cases} N_{n,l}^o \text{Ms}_l^{(1)}(u, q_{1,n,l}) \text{se}_l(v, q_{1,n,l}), & u \leq U, \\ N_{n,l}^o \text{Ms}_l^{(3)}(u, -q_{2,n,l}) \text{se}_l(v, -q_{2,n,l}), & u > U, \end{cases} \quad (12)$$

where $N_{n,l}^e$ and $N_{n,l}^o$ are determined by normalization of the complete wave function.

III. NUMERICAL RESULTS

In Fig. 2 we show the dependence of the energy of the bound states on the strength of the well $\gamma = \sqrt{\frac{2m}{\hbar^2} abV_0}$, which depends both on the potential height V_0 and on the area of the dot ab . For clarity we have limited all our graphs to $l \leq 7$. For $a/b = 1$ the results coincide with our calculations for a circular dot. When the ratio a/b increases, the degeneracy of the $l \neq 0$ energy levels is lifted and they split in separate levels. This is a result of a decrease in symmetry of the system in the transition from a circular to an elliptic dot. With increasing a/b , energy levels corresponding with even states lower, while those corresponding with uneven states rise in energy. This behavior is more clearly visible in Fig. 3, where we have plotted the energy levels against the ratio a/b , with γ fixed. For small and narrow dots, only the even $n = 1$ states remain, while the uneven states become unbound. The total number of states stays approximately equal. In Fig. 3 it is also clear that even the smallest and narrowest dot holds at least one confined state. The energy of this lowest state is shown in Fig. 4 as a function of the eccentricity a/b . There is only a small increase of the energy level with increasing eccentricity.

The asymptotic behavior for the energy of the ground state in a shallow 2D well can be obtained analytically. Because of the weak dependence of this energy on the eccentricity we assume for simplicity $a/b = 1$. Outside the well the wavefunction is then given by the modified Bessel function,

$$\Psi(\rho) = K_0 \left(\sqrt{\frac{2m}{\hbar^2} |E_0|} \rho \right), \quad (13)$$

where $|E_0| = V_0 - E$ is the binding energy in the well and $\rho = (x^2 + y^2)^{1/2}$. For small $|E_0|$ this wave function can to first order be approximated by

$$\Psi(\rho) \approx -\ln\left(\frac{e^g}{2}\sqrt{\frac{2m}{\hbar^2}}|E_0|\rho\right), \quad (14)$$

with $g = 0.57721 \dots$ the constant of Euler-Mascheroni. Inside the potential well the ground state wave function is almost constant. Integrating this function over the Schrödinger equation we obtain the binding energy

$$|E_0| = \frac{4}{e^{2g}} \frac{\hbar^2}{2ma^2} \exp\left(-\frac{2\hbar^2}{mV_0a^2}\right) \quad (15)$$

with the prefactor $4/e^{2g} = 1.26096 \dots$. In Figs. 2 and 3 the ground state energy for small γ can be approximated by

$$E/V_0 = 1 - \frac{1.26}{\gamma^2} e^{-4/\gamma^2}. \quad (16)$$

The results for an infinitely high confinement potential are shown in Fig. 5. The behavior is comparable to the finite well case, except that all the energy levels will eventually rise with increasing eccentricity.

Notice that in Fig. 5 we find that for large eccentricity the energy levels appear in bands where the levels are practically equidistant. This can be understood from the following simple consideration. If $b/a \ll 1$ we can use an adiabatic approximation and assume that the motion along the y -direction is much faster than along x . For $|x| < a$ the electron feels a hard wall potential along the y -direction of width $W = 2b\sqrt{1-x^2/a^2}$ which has energy levels $E_y = \frac{\pi^2\hbar^2}{2mW}n_y^2$. This results into a potential along the x -direction $V(x) = \frac{\pi^2\hbar^2}{8mb^2} \frac{n_y^2}{(1-x^2/a^2)} \simeq \frac{\pi^2\hbar^2}{8mb^2}n_y^2(1+x^2/a^2)$ which near its minimum is parabolic. The resulting energy levels become $E_{n_x, n_y} = \frac{\pi^2\hbar^2}{8mb^2}n_y^2 + \frac{\pi^2\hbar^2}{2mab}n_y(n_x + 1/2)$, which for fixed n_y results into an equidistant set of levels as found in Fig. 5 for $a/b \gg 1$. The dependence on the eccentricity becomes more clear if we introduce $\sigma = \sqrt{ab}$, which was taken fixed in Fig. 5, into the above expression, which leads to

$$E_{n_x, n_y} = \frac{\pi^2\hbar^2}{8m\sigma^2}n_y^2\frac{a}{b} + \frac{\pi^2\hbar^2}{2m\sigma^2}n_y(n_x + 1/2). \quad (17)$$

Notice that the linear increase with a/b results from the zero point motion along the y -direction.

To see the effect of different well (m_1) and barrier (m_2) masses we present in Fig. 6 the results for the bound states in the case of three different mass ratios $\mu = m_2/m_1 = 0.5, 1$ and 2. There is a decrease of the energy levels, i.e. increase of binding, when the effective mass of the electron outside the dot is higher than inside the dot. The $l = 0$ levels become bound at the same value for γ , while this is no longer the case for $l > 0$.

The density distribution of the wave functions corresponding to the different bound states, denoted by $(n, l)^e$ or $(n, l)^o$, are shown in Fig. 7 for $a/b = 5$ and $\gamma = 11$. The even $n = 1$ states form the lowest levels and they have all their extrema of the wave function located along a row in the direction of the longest axis of the ellipse. In this particular case, a second row of extrema appears only at the sixth state $(1, 1)^o$, which is odd. When $n = 2$, we see three rows appear. In all cases the number of extrema in a row is determined by l . The general pattern is that the lowest levels are those for which the position of the extrema of the wave function best fit the shape of the quantum dot.

IV. CONCLUSIONS

By expressing the wave functions in the appropriate coordinate system, viz. elliptical coordinates, we were able to find analytical solutions for the Schrödinger equation describing an elliptical quantum dot with finite height hard walls. These functions are the Mathieu functions. The condition of smoothness of the wave function at the boundary of the dot, results in an expression for the energy levels. The main effect of the elongation of the dot from a circular to an elliptic shape is a lifting of the degeneracy of the $l > 1$ levels. We found exact results for the energy levels and the wave functions for arbitrary quantum numbers. The basic solutions found here may be the basis for more advanced problems with elliptic geometry, e.g. many particle quantum dots and quantum dots in a magnetic field. The results can readily be expanded to the case of an elliptic wire. The particle can then move freely along the z -direction of a wire with an elliptic cross-section. For the energy states we find

$$\tilde{E}_{n,l,k_z} = \frac{\hbar k_z^2}{2m} + E_{n,l}, \quad (18)$$

where $E_{n,l}$ are the above discussed levels and the wave functions are

$$\tilde{\Psi}(x, y, z) = e^{ik_z z} \Psi_{n,l}(x, y). \quad (19)$$

ACKNOWLEDGMENTS

This work was supported by the Flemish Science Foundation (FWO-VI), IUAP-IV, and the "Bijzonder Onderzoeksfonds van de Universiteit Antwerpen". F. M. P. acknowledges discussions with J. M. Worlock in the initial stage of this work.

APPENDIX

Solutions to Eq. (3b) are found in the form of a Fourier series. Physically relevant solutions obey periodic boundary conditions

$$G(v) = G(v + \pi), \quad (A.1a)$$

$$G(v) = G(v + 2\pi). \quad (A.1b)$$

Even periodic solutions are expanded in a Fourier series of cosine functions, while odd periodic solutions are expanded in a Fourier series of sine functions. In this way, we find the four fundamental solutions, which are called the Mathieu functions [14–16]

$$ce_{2l}(v, q) = \sum_{j=0}^{\infty} A_{2j}^{2l}(q) \cos 2jv, \quad (A.2a)$$

$$ce_{2l+1}(v, q) = \sum_{j=0}^{\infty} A_{2j+1}^{2l+1}(q) \cos(2j+1)v, \quad (A.2b)$$

$$se_{2l+1}(v, q) = \sum_{j=0}^{\infty} B_{2j+1}^{2l+1}(q) \sin(2j+1)v, \quad (\text{A.2c})$$

$$se_{2l+2}(v, q) = \sum_{j=0}^{\infty} B_{2j+2}^{2l+2}(q) \sin(2j+2)v. \quad (\text{A.2d})$$

By substituting these series into Eq. (3b), we find a set of recursion relations for the expansion coefficients, e.g. for $A_{2j}^{2l}(q)$

$$\begin{aligned} cA_0^{2l} - qA_2^{2l} &= 0, \\ (c-4)A_2^{2l} - q(2A_0^{2l} + A_4^{2l}) &= 0, \\ [c - (2l)^2]A_{2j}^{2l} - q(A_{2j-2}^{2l} + A_{2j+2}^{2l}) &= 0 \quad (j \geq 2). \end{aligned} \quad (\text{A.3})$$

Numerical methods to calculate the Mathieu functions are described in detail in the literature [9–13,15]. Solutions to Eq. (3a) are written as an expansion in Bessel functions. With $u_1 = \sqrt{q}e^{-u}$ and $u_2 = \sqrt{q}e^u$ we find

$$\text{Mc}_{2l}^{(1)}(u, q) = \frac{1}{A_0^{2l}(q)} \sum_{j=0}^{\infty} (-1)^{j+l} A_{2j}^{2l}(q) J_j(u_1) J_j(u_2), \quad (\text{A.4a})$$

$$\text{Mc}_{2l+1}^{(1)}(u, q) = \frac{1}{A_1^{2l+1}(q)} \sum_{j=0}^{\infty} (-1)^{j+l} A_{2j+1}^{2l+1}(q) [J_j(u_1) J_{j+1}(u_2) + J_{j+1}(u_1) J_j(u_2)], \quad (\text{A.4b})$$

$$\text{Ms}_{2l+1}^{(1)}(u, q) = \frac{1}{B_1^{2l+1}(q)} \sum_{j=0}^{\infty} (-1)^{j+l} B_{2j+1}^{2l+1}(q) [J_j(u_1) J_{j+1}(u_2) - J_{j+1}(u_1) J_j(u_2)], \quad (\text{A.4c})$$

$$\text{Ms}_{2l+2}^{(1)}(u, q) = \frac{1}{B_2^{2l+2}(q)} \sum_{j=0}^{\infty} (-1)^{j+l} B_{2j+2}^{2l+2}(q) [J_j(u_1) J_{j+2}(u_2) - J_{j+2}(u_1) J_j(u_2)], \quad (\text{A.4d})$$

and

$$\text{Mc}_{2l}^{(3)}(u, -q) = \frac{2i}{\pi} \frac{(-1)^{l+1}}{A_0^{2l}(q)} \sum_{j=0}^{\infty} A_{2j}^{2l}(q) I_j(u_1) K_j(u_2), \quad (\text{A.5a})$$

$$\text{Mc}_{2l+1}^{(3)}(u, -q) = \frac{2}{\pi} \frac{(-1)^{l+1}}{B_1^{2l+1}(q)} \sum_{j=0}^{\infty} B_{2j+1}^{2l+1}(q) [I_j(u_1) K_{j+1}(u_2) - I_{j+1}(u_1) K_j(u_2)], \quad (\text{A.5b})$$

$$\text{Ms}_{2l+1}^{(3)}(u, -q) = \frac{2}{\pi} \frac{(-1)^{l+1}}{A_1^{2l+1}(q)} \sum_{j=0}^{\infty} A_{2j+1}^{2l+1}(q) [I_j(u_1) K_{j+1}(u_2) + I_{j+1}(u_1) K_j(u_2)], \quad (\text{A.5c})$$

$$\text{Ms}_{2l+2}^{(3)}(u, -q) = \frac{2i}{\pi} \frac{(-1)^l}{B_2^{2l+2}(q)} \sum_{j=0}^{\infty} B_{2j+2}^{2l+2}(q) [I_j(u_1) K_{j+2}(u_2) - I_{j+2}(u_1) K_j(u_2)]. \quad (\text{A.5d})$$

To obtain the derivatives of the Mathieu functions we used these series expansions of the Mathieu functions and applied the analytical formulas for the derivatives of Bessel functions [14].

REFERENCES

- * Electronic address: francois.peeters@ua.ac.be
- [1] See, for example, *Quantum Dots*, Eds. L. Jacak, P. Hawrylak, and A. Wojs, (Springer-Verlag, Berlin, 1998).
 - [2] F. M. Peeters and V. A. Schweigert, Phys. Rev. B **53**, 1468 (1996).
 - [3] J. M. Worlock, F. M. Peeters, H. M. Cox and P. C. Morais, Phys. Rev. B **44**, 8923 (1991).
 - [4] G. W. Bryant, in *Interfaces, Quantum Wells, and Superlattices*, Eds. by C. R. Leavens and R. Taylor (Plenum Press, New York, 1988), p. 143.
 - [5] D. Gershoni, H. Temkin, G. J. Dolan, J. Dunsmuir, S. N. G. Chu and M. B. Panish, Appl. Phys. Lett. **53**, 995 (1988).
 - [6] P. M. Morse and P. J. Rubenstein, Phys. Rev. **54**, 895 (1938).
 - [7] S. Granger and R. D. Spence, Phys. Rev. **83**, 460 (1951).
 - [8] G. Cantele, D. Ninno and G. Iadonisi, J. Phys.: Condens. Matter **12**, 9019 (2000).
 - [9] F. A. Alhargan, SIAM Rev. **38**, 239 (1996).
 - [10] W. R. Leeb, ACM Trans. Math. Softw. **5**, 112 (1979).
 - [11] R. B. Shirts, ACM Trans. Math. Softw. **19**, 377 (1993).
 - [12] R. B. Shirts, ACM Trans. Math. Softw. **19**, 391 (1993).
 - [13] A. Lindner and H. Freese, J. Phys. A **27**, 5565 (1994).
 - [14] M. Abramowitz and I. A. Stegun, *Handbook of Mathematical Functions* (Dover, New York, 1968), Chpt. 20 and Chpt 9.
 - [15] S. Zhang and J. Jin, *Computation of Special Functions*, (Wiley, New York, 1996), Chpt. 14.
 - [16] P. M. Morse and H. Feshbach, *Methods of Theoretical Physics*, (McGraw-Hill, New York, 1953), p. 633 and p. 1407.

FIGURES

FIG. 1. The potential profile $V(x, y)$ is zero inside the elliptic dot and equal to V_0 outside the dot. The long axis of the ellipse is $2a$, the short axis is $2b$.

FIG. 2. The confined even and odd states $(n, l)^{e/o}$ of an elliptic quantum dot with eccentricity a/b as a function of the strength of the well γ . All dots have at least one bound state. (a) For $a/b = 1$ the even and odd states are degenerate. (b) When $a \neq b$ this degeneracy is lifted for $l > 0$.

FIG. 3. The confined energy states $(n, l)^{e/o}$ of an elliptic quantum dot with strength $\gamma = 9$ as a function of the eccentricity a/b . All the even $n = 1$ states decrease with increasing a/b .

FIG. 4. The energy of the ground state $(1, 0)^e$ of shallow elliptic quantum dots with small strengths $\gamma = 1, 1.5, 2, 3$ and 4 as a function of the eccentricity a/b .

FIG. 5. The energy states in an infinite elliptic quantum well as a function of the eccentricity a/b . The effective electron mass was taken to be $m^* = 0.041 m_e$ and the area of the dot $\sigma = (ab)^{1/2} = 10$ nm.

FIG. 6. The confined energy states of an elliptic quantum dot with eccentricity $a/b = 5$ as a function of the strength of the well γ for different mass ratio $\mu = m_2/m_1$ where m_1 (m_2) is the effective mass of the electron inside (outside) the dot. For clarity we have split up the graph for different l .

FIG. 7. The probability density for the eigenfunctions $(n, l)^{e/o}$ of all the bound states in an elliptic quantum dot with strength $\gamma = 11$ and ratio $a/b = 5$ in order of increasing energy. The lowest states have $n = 1$ and are all even: the maxima in the probability are along the long axis of the ellipse. Only higher energy states can have more rows of maxima.

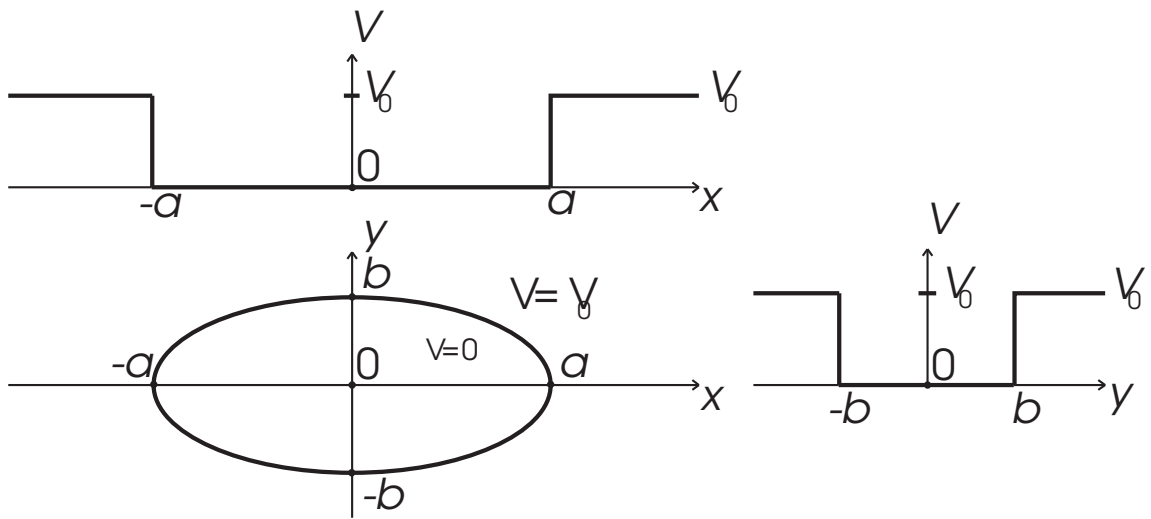


FIG 1: M. VAN DEN BROEK AND F. M. PEETERS

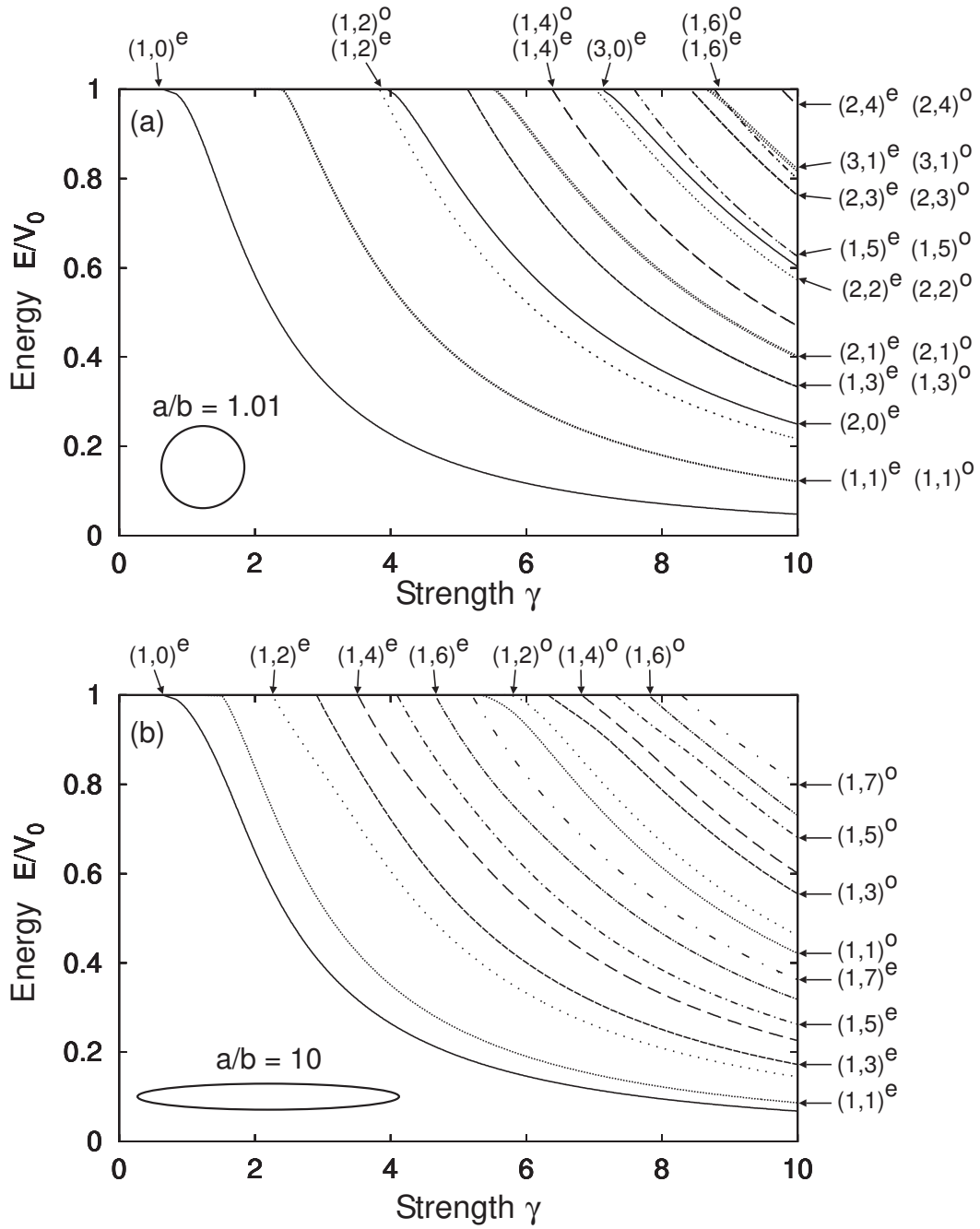


FIG 2: M. VAN DEN BROEK AND F. M. PEETERS

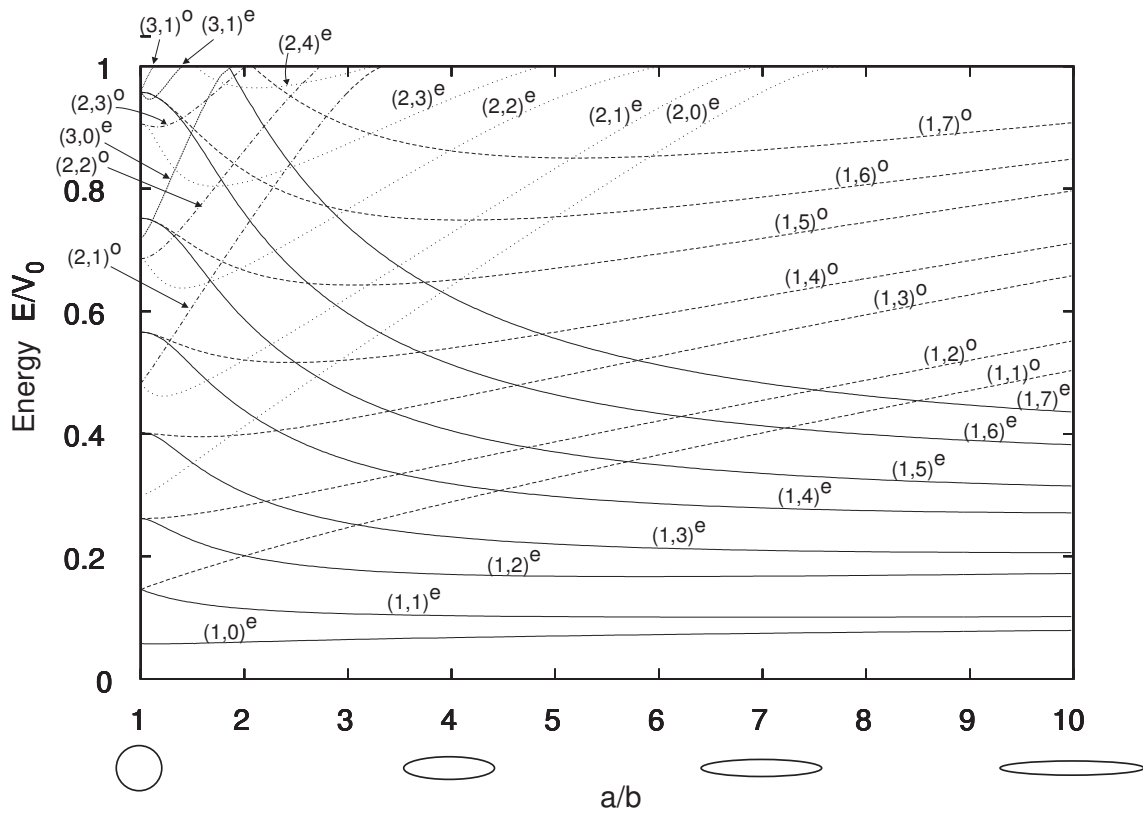


FIG 3: M. VAN DEN BROEK AND F. M. PEETERS

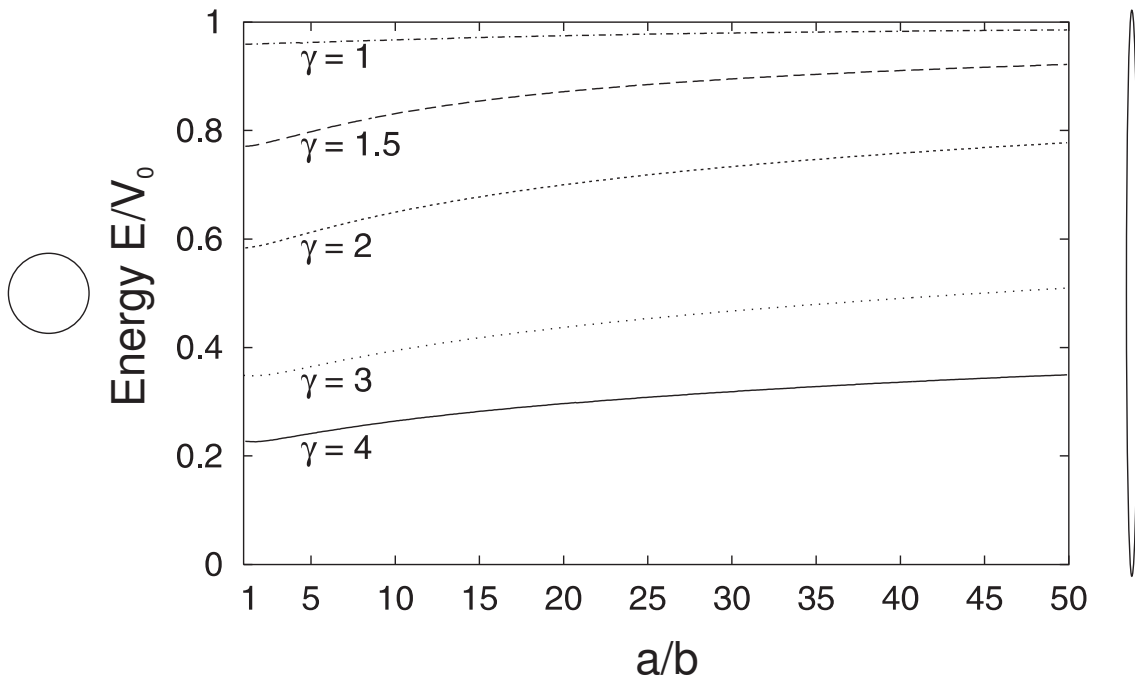


FIG 4: M. VAN DEN BROEK AND F. M. PEETERS

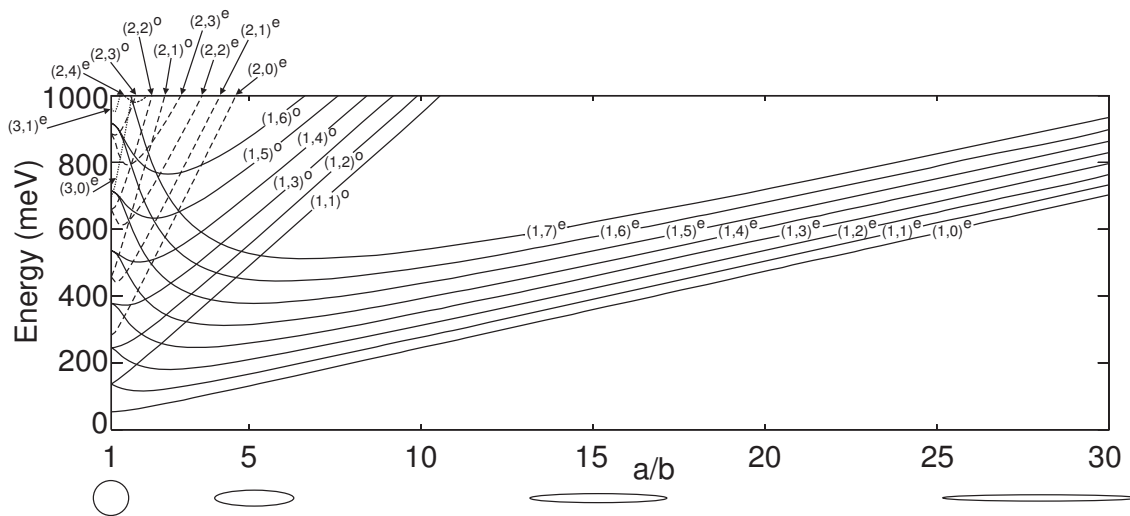


FIG 5: M. VAN DEN BROEK AND F. M. PEETERS

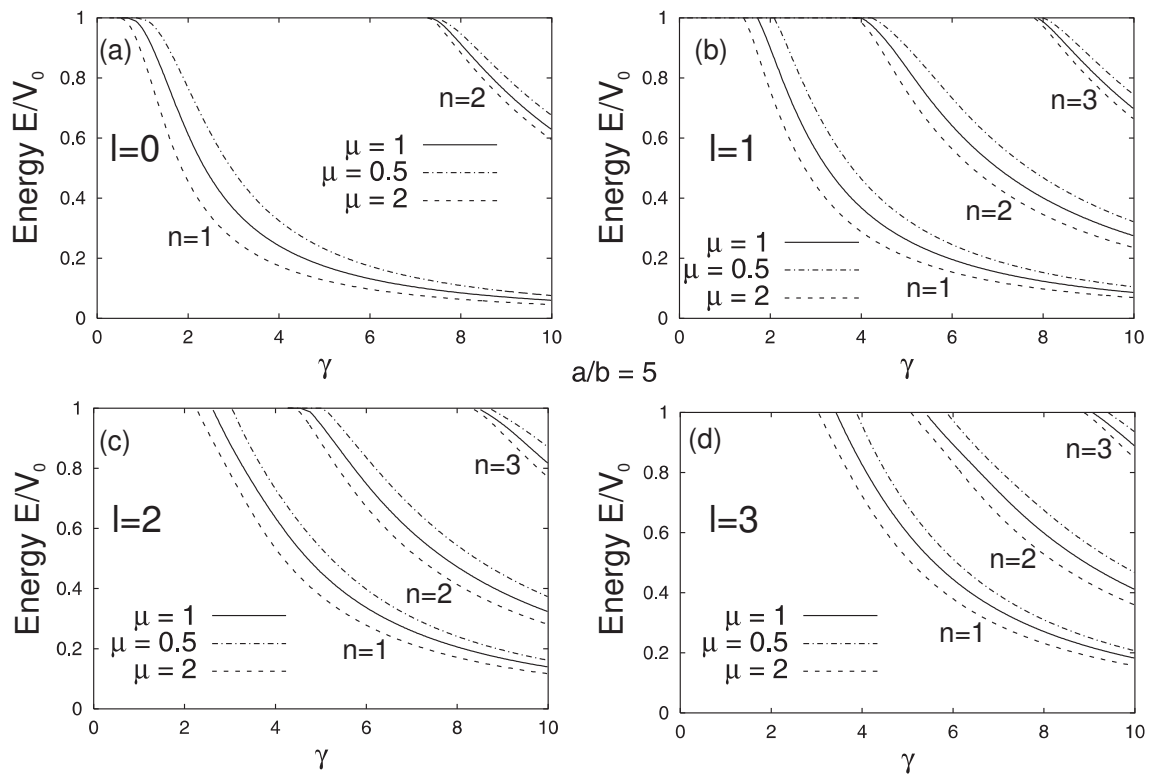


FIG 6: M. VAN DEN BROEK AND F. M. PEETERS

This figure "fig7a.jpg" is available in "jpg" format from:

<http://arxiv.org/ps/cond-mat/0107321v2>

This figure "fig7b.jpg" is available in "jpg" format from:

<http://arxiv.org/ps/cond-mat/0107321v2>